Composition and structure of porcine digital flexor tendon-bone insertion tissues

Sandhya Chandrasekaran, Mark Pankow, Kara Peters, Hsiao-Ying Shadow Huang iD

Department of Mechanical and Aerospace Engineering, North Carolina State University, R3158 Engineering Building 3, Campus Box 7910, 911 Oval Drive, Raleigh, North Carolina 27695, USA

Abstract: Tendon-bone insertion is a functionally graded tissue, transitioning from 200 MPa tensile modulus at the tendon end to 20 GPa tensile modulus at the bone, across just a few hundred micrometers. In this study, we examine the porcine digital flexor tendon insertion tissue to provide a quantitative description of its collagen orientation and mineral concentration by using Fast Fourier Transform (FFT) based image analysis and mass spectrometry, respectively. Histological results revealed uniformity in global collagen orientation at all depths, indicative of mechanical anisotropy, although at mid-depth, the highest fiber density, least amount of dispersion, and least cellular circularity were evident. Collagen orientation distribution obtained through 2D FFT of histological imaging data from fluorescent microscopy agreed with past measurements based on polarized light microscopy. Results revealed global fiber orientation across the tendon-bone insertion to be preserved along direction of physiologic tension. Gradation in the fiber distribution orientation index across the insertion was reflective of a decrease in anisotropy from the tendon to the bone. We provided elemental maps across the fibrocartilage for its organic and inorganic constituents through time-of-flight secondary ion mass spectrometry (TOF-SIMS). The apatite intensity distribution from the tendon to bone was shown to follow a linear trend, supporting past results based on Raman microprobe analysis. The merit of this study lies in the image-based simplified approach to fiber distribution quantification and in the high spatial resolution of the compositional analysis. In conjunction with the mechanical properties of the insertion tissue, fiber, and mineral distribution results for the insertion from this may potentially be incorporated into the development of a structural constitutive approach toward computational modeling. Characterizing the properties of the native insertion tissue would provide the microstructural basis for developing biomimetic scaffolds to recreate the graded morphology of a fibrocartilaginous insertion. © 2017 Wiley Periodicals, Inc. J Biomed Mater Res Part A: 00: 000–000, 2017.

Key Words: tendon-bone insertion, collagen fiber orientation, fast fourier transform, time-of-flight secondary ion mass spectrometry

INTRODUCTION

Orthopedic junctions such as tendon-bone insertions are complex transitional tissues responsible for load transfer between soft tissues and bone, and are susceptible to injury due to stress concentrations.[1–4] Native tendon-bone insertion tissues may be fibrous or fibrocartilaginous in nature.[5] At the injury-prone attachment sites of the Achilles and rotator cuff tendons, the insertion is an inhomogeneous fibrocartilage that is graded structurally and functionally. In particular, the tendon end is characterized by highly aligned collagen fibers, while the hard bone end is characterized by the mineral hydroxyapatite.[2,3,6–10] However, following suture-based surgical fixation of ruptured tendons back to the bone site, the regenerating insertion is a disorganized fibrovascular scar marked by discontinuity in both the collagen microstructure and the mineral distribution and thereby, susceptible to reinjury.[8,11,12] For the purpose of developing tissue-engineered constructs to reproduce the physiologic heterogeneity during regeneration, it is critical to understand the natural structure-function properties by integrating the mechanical behavior of the tissue with its microstructure and biochemical composition.

Unlike fibrous insertions in healing tissues, native fibrocartilaginous insertions consist of four distinct zones which have been categorized based on their extracellular matrix composition.[2,3,9] Tendon tissue itself is characterized by type I collagen and tendon-specific proteoglycans, namely decorin and biglycan. At the insertion, tendon transitions into fibrocartilage where types II and III collagen are expressed along with lesser amounts of types I, IX, and X. Towards the bony end of the fibrocartilage, there is a well-defined mineralization front expressing cartilage specific proteoglycan namely, aggrecan, and significant amount of types II and X collagen. The pure bone region is again rich

Correspondence to: H.-Y. S. Huang; e-mail: hshuang@ncsu.edu

in type I collagen. Aligned tendon fibers insert into bone by means of continuous gradation in both the collagen fiber direction as well as the mineral concentration,[7,13,14] allowing them to resist pull-out and prevent stress concentration.

In the context of tendon-bone load transfer, previous studies have investigated geometric and morphological effects on computational stress singularities occurring at the interface of two dissimilar materials.[15,16] Using finite element analyses of idealized insertions, spatial variation of the mean orientation angle of the collagen fiber distribution was shown to have a strong effect on principal stresses and the locations of stress concentrations.[10] Mechanical orthotropy (defined as maximum to minimum tensile stiffness) was shown to vary by about 50% over the entire insertion, pointing to the fact that the angular deviation of collagen fibers dictated the directional variation in stiffness. One of the objectives in this study was to examine and quantitatively measure the orientation of collagen fibers along the insertion tidemark and to examine how the native fiber distribution compares to the idealized isotropic, orthotropic, physiologic, and optimized models mentioned in previous studies.[10]

Collagen fiber distribution studies have used quantitative and/or qualitative techniques such as polarized light microscopy,[17,18] small angle light scattering,[19–23] fluorescent microscopy,[24] optical coherence microscopy,[25] electron microscopy,[26] and second harmonic generation microscopy.[27] However, the small angle light scattering requires a laser technique for measuring the collagen fiber distribution. It suffers from several difficulties, such as the setup of the equipment is time consuming and requires a relatively large dedicated space. Optical coherence microscopy is much more expensive and the required tissue sample is bigger than the insertion tissue. Electron microscopy and second harmonic generation microscopies require addition sample preparations, such as critical point drying or freeze dry, resulting in sample shrinkage or tearing, respectively. Fiber organization at supraspinatus insertions in rats was measured[2,3] using polarized light microscopy, taking advantage of collagen birefringence.[18] Tissue sections placed on a stage between a simultaneously rotating analyzer and polarizer were imaged using a microscope camera. The angle of minimum light intensity during the incremental rotation, known as the extinction angle, indicated the orientation of collagen fibers. This study attempts to overcome the need for a polarized light microscopy set-up by utilizing histology image data for the quantitative fiber study at the insertion tissue.

To quantify the collagen fibers architecture and morphology on two orthogonal planes of the insertion tissue, we apply 2D Fast Fourier Transform (FFT)[28–30] of histological image data from fluorescent microscopy. FFT-based methods have been used in image analysis to study fiber architecture in biomimetic scaffolds,[30,31] collagen structure in corneal stroma,[27] aortic aneurysms,[32] and arteries.[33] These methods are also incorporated as plug-ins in the Image J and Fiji image analysis softwares.[34,35] The FFT method in conjunction with a band pass filter has been shown to give more accurate results for orientation and dispersion parameters of fiber networks in comparison to gradient-based structural tensor methods, which have been used in the past for fiber distribution studies in arterial adventitia[36] and actin filaments in the lamellipodium.[37] Although image analyses using FFT have been performed to study collagen structure of soft tissues,[27,35] this technique has not been previously applied to study fiber direction evolution across the tendon-to-bone insertion.

Histological studies showed evidence of fiber dispersion away from the tendon axis at the unmineralized fibrocartilage as well as anchoring of the fibers into bone at the fibrocartilage mineralization front.[2,3,7,10] Previous studies[13,14] have examined the microscale spatial distribution of mineralization across murine rotator cuff insertions using Raman microprobe analysis. The abundance of mineral and collagen at any point was measured based on the intensity of peaks corresponding to the P-O stretch from calcium hydroxyapatite $(Ca_{10}(PO_4)_6(OH)_2)$ and the C-C stretch from the collagen protein, respectively. The spectral information was obtained on a discrete basis at selected points. Complementarily, time-of-flight secondary ion mass spectrometry (TOF-SIMS)[38–47] can be used to obtain spatially continuous molecular mapping from the upper most monolayer of the tissue. In the past 20 years, TOF-SIMS has been a widely used surface analysis technique for obtaining high-quality spectra owing to its combination of high mass-resolution ($>10,000$ M/ΔM), mass range (0–10,000 amu), spatial resolution (<300 nm), and simultaneous molecular mapping.

In the past, TOF-SIMS has been used for investigating biological tissues for unknown molecules,[42,45,46] polymer characterization,[47] and for identifying impurities on biomaterial surfaces of medical implants.[41] The high surface sensitivity is attributed to the collision cascade energy (in the keV range) being just sufficient for molecular bond-breaking within the top 1–2 nm. Hydroxyapatite and other biomedically relevant calcium-phosphate phases have been previously characterized using this technique.[43,44] For example, traces of biomineralization were identified based on calcium-phosphate deposits on the skin surface of a mummy sample[42] using TOF-SIMS. In the current study, we examine the organic and inorganic constituents of the insertion fibrocartilage based on the intensity distributions of apatite and collagen protein fragments at the porcine digital flexor tendon insertion.

The peculiarity of the insertion tissue arises from its gradations in fiber direction and mineral concentration. This study provides quantitative spatial descriptions of both these properties. First, through fluorescence microscopy of Hematoxylin and Eosin (H&E)-stained sections, the microstructure of the insertion tissue is examined along two orthogonal planes. The corresponding fluorescent images are analyzed based on FFT to obtain fiber orientation information across and along the insertion boundary. Second, a continuous description of the apatite concentration and of collagen protein is provided based on surface mass spectrometry using TOF-SIMS.
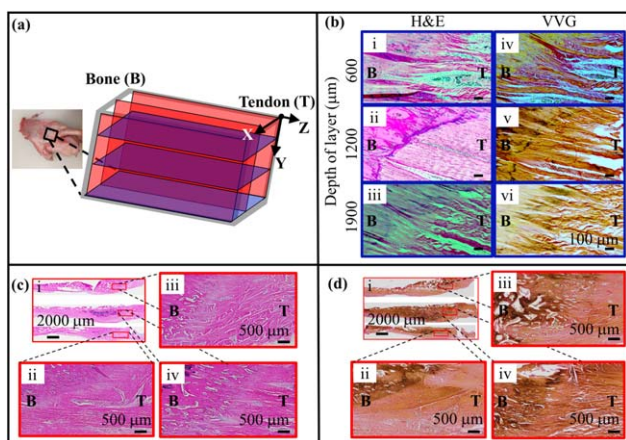
FIGURE 1. (a) Histological slides were prepared from different depths in the horizontal plane (X-Z) and the sagittal plane (Y-Z) in the porcine digital flexor tendon insertion tissue. Brightfield images at 400× magnification (water immersion) obtained using a Zeiss Axioimager (Zeiss Inc., Germany) microscope for (b. i–iii) sections on X-Z planes using H&E staining, (b. iv–vi) VVG staining (scale bar = 100 μm), (c) sections on Y-Z planes using H&E and (d) VVG staining. Qualitatively, fiber orientation in the X-Z plane in (b) is centered around the direction of physiological tension. The section at mid-depth (b.ii) reveals maximum fiber density, the least amount of dispersion, and the least cellular circularity. Closer to the surface, there is lower fiber density and organization, accompanied by the increased presence of proteoglycans and cellular circularity. It is evident from (d.ii) in the Y-Z plane that the collagen fibers are deviating away from the tendon axis and toward the normal to the curved insertion boundary.

This study addresses the quantification of collagen structure through FFT image analysis and provides a fast and accurate alternative to the polarized light microscopy method, as well as characterizing the mineral composition through high spatial resolution spectral analysis using TOF-SIMS. The combination of both of these structural aspects forms the basis for understanding the interconnection of the collagen fiber structure with the mineralization network at the insertion tissue to assist with designing effective biomimetic surfaces.

METHODS
Sample preparation
Digital flexor tendon-bone units were removed from porcine forelimbs procured from the local abattoir. We chose to work with the digital flexor tendon is due to that it is one of the larger insertion tissues that is easy to obtain. Two samples were preserved for microscopy in 10% buffered formalin under zero tension over 2–3 days prior to dehydration and decalcification. Specimens were processed for standard paraffin embedded histology and sectioned in both the horizontal (X-Z) and sagittal planes (Y-Z), as shown in the schematic in Figure 1(a). In the horizontal plane, 25 μm thick sections were obtained at 25 μm intervals throughout the depth of the insertion tissue [blue planes in Fig. 1(a)] and in the sagittal plane, 25 μm thick sections were obtained at 50 μm intervals along the x-axis [or the mediolateral direction indicated by red planes in Fig. 1(a)].

For the purpose of the TOF-SIMS analysis, three samples were preserved in Hank's Balanced Salt Solution at 4°C

prior to sectioning. 100 μm thick frozen samples sectioned in the X-Z plane of tendon insertion were obtained at −20°C using a clinical cryostat (Leica CM1950, Leica, Wetzlar, Germany) and the unstained, unfixed samples were mounted on glass slides. After intermediate storage at 4°C, the sections were left for freeze drying in the vacuum chamber of the TOF-SIMS 24 h prior to the actual analysis.

Fiber microstructure and orientation distribution
Image generation. Brightfield images at 400× magnification (water immersion) were obtained using the Zeiss Axioimager (Zeiss Inc., Germany) microscope at the Cellular and Molecular Imaging Facility at North Carolina State University. The collagen structures of both planes were imaged using H&E staining and Verhoeff-Van Geison (VVG) staining, respectively.

For image analysis using FFT, intrinsic fluorescence of the H&E stain (i.e., the eosin dye) was being utilized for the FFT-based orientation analysis and sections at mid-depth in the horizontal and sagittal planes [shown in Fig. 1(b-ii,c-iv), respectively] were imaged using a GFP fluorescence filter set (excitation wavelength = 450–490 nm and emission wavelength = 500–550 nm) at a 40× objective (water immersion) [Fig. 2(a)]. Image analysis was performed after cropping out the three regions of interest, namely pure bone, insertion, and pure tendon, as shown in Figure 2(b) and five different regions along the insertion boundary as shown in Figure 3(b,c). Mean fiber orientation angle on each image is indicated by α, and angle of normal to the curved insertion boundary (that is, tidemark) is indicated by β.

Image processing using FFT. Images from fluorescent microscopy were converted from RGB to grayscale before converting to the frequency domain by applying 2D discrete Fourier transformation as shown in Eq. (1) by using the *fft2* function in a custom MATLAB (2016b, MathWorks, Natick, MA) script:[31]

$$F(u,v) = \sum_{x=1}^{M} \sum_{y=1}^{N} f(x,y) e^{-i2\pi\left(\frac{ux}{M}\right) - i2\pi\left(\frac{vy}{N}\right)} \tag{1}$$

In Eq. (1), x and y denote the pixel coordinates on the image while u and v denote the frequencies corresponding to changes in the pixel intensity across the image spatial coordinates. Total pixel count is given by $M \times N$ for each of the cropped images in Figure 2(b). For example, in the tendon region (T) the pixel count is 112×112. The simplistic case of the regularly spaced alternating black and white stripes on an image would correspond to a single harmonic frequency. The actual image being analyzed is thus the inverse transformation of the superposition of such frequencies in the x and y-directions.

The *fftshift* function is applied to the Fourier transform to cluster the zero-frequency component in the middle of the spectrum. The transform is converted to a log spectrum of its magnitude to eliminate its imaginary component. By
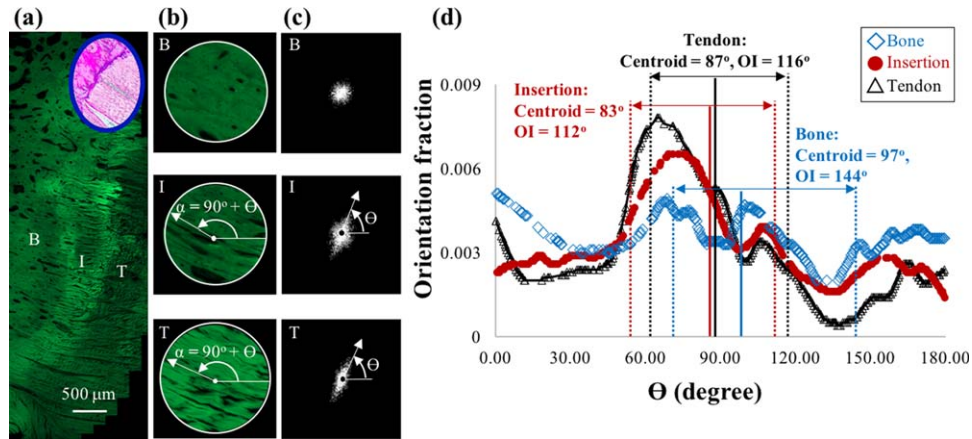
FIGURE 2. (a) H&E stained section in the X-Z plane was used for measurement of collagen fiber orientation in the bone (B), insertion (I), and tendon (T) regions. Fluorescent microscopy of the section was conducted using a GFP fluorescence filter set (excitation wavelength 450–490 nm, emission wavelength 500–550 nm) at 400× magnification (water immersion), (b) Mean fiber orientation is represented by α in the cropped images, (c) FFT was applied to the cropped images. Angle of orientation of the white pixels on the FFT image is represented by Θ. (d) Orientation distribution based on FFT image pixels reveals similar angles of fiber orientation in the insertion and tendon regions. OI decreases from bone to tendon, suggesting a decrease in fiber dispersion and an increase in anisotropy, in agreement with previous results based on polarized light microscopy.[2,3]

means of noise filtering, the spectrum is shifted by its minimum value for the initial value to be zero and scaled down by its highest value to produce the FFT as shown in Figure 2(c). The angle of orientation of white pixels on the FFT image is represented by Θ.

Orientation distribution. Fiber orientation distribution is interpreted based on the angular distribution of FFT image pixels. By fitting the FFT image pixel data onto a circular distribution, the number of pixels oriented along each incremental angle from 0 to π is obtained. The count of FFT image pixels associated with each incremental angle is baseline corrected using the minimum value and the result is normalized as a fraction of the maximum value. By numerical integration, the total area under angular distribution of

the normalized pixel count is obtained. Each individual pixel count is further normalized by the total area to obtain the unit area orientation distribution as shown in Figure 2(d). It should be noted that the orientation distribution corresponds to the angular orientation of the FFT image pixels with respect to the indicated coordinate system [Fig. 2(c)]. Mean angles of orientation associated with each of the three regions of interest are calculated as the angles corresponding to the centroids of the respective distributions. Hence, the peak angle in each distribution corresponds to the direction of highest frequency content and is presumably 90° out of phase with the orientation of the fibers in the cropped images in Figure 2(b). For example, in the tendon region (T), the angle on the FFT (Θ) corresponding to a peak value of orientation distribution is 87° as seen in
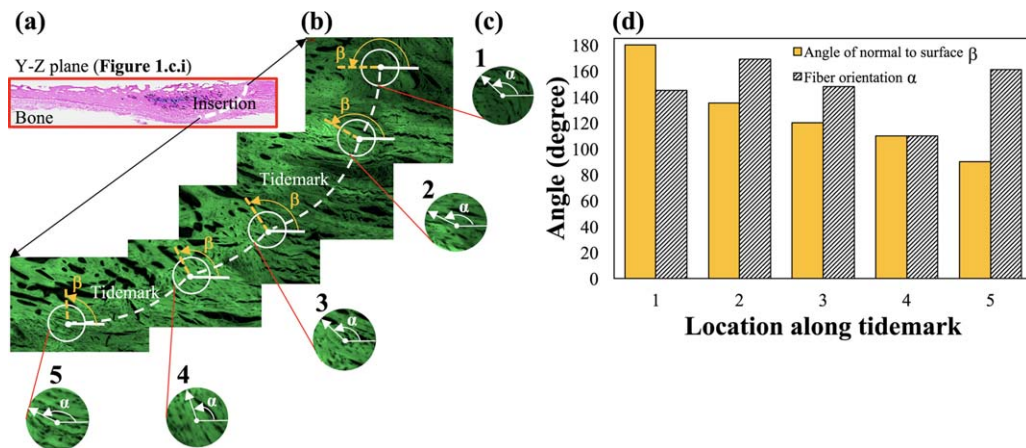

FIGURE 3. (a) H&E stained section in the Y-Z plane was used for measurement of collagen fiber orientation. (b) A stained tissue section was imaged using a GFP fluorescence filter set (excitation wavelength 450–490 nm, emission wavelength 500–550 nm) at 400× magnification (water immersion). The angle of orientation of the normal to the curved insertion boundary is indicated as β. (c) Regions of interest for image analysis were cropped out along the insertion boundary. Mean fiber orientation is represented by α. (d) Fiber rotation in the curved boundary was studied based on deviation of collagen fiber direction from the tendon axis (0°). The results indicate that the normal to the insertion boundary is not necessary parallel with the collagen fiber orientation α of tendon tissue.
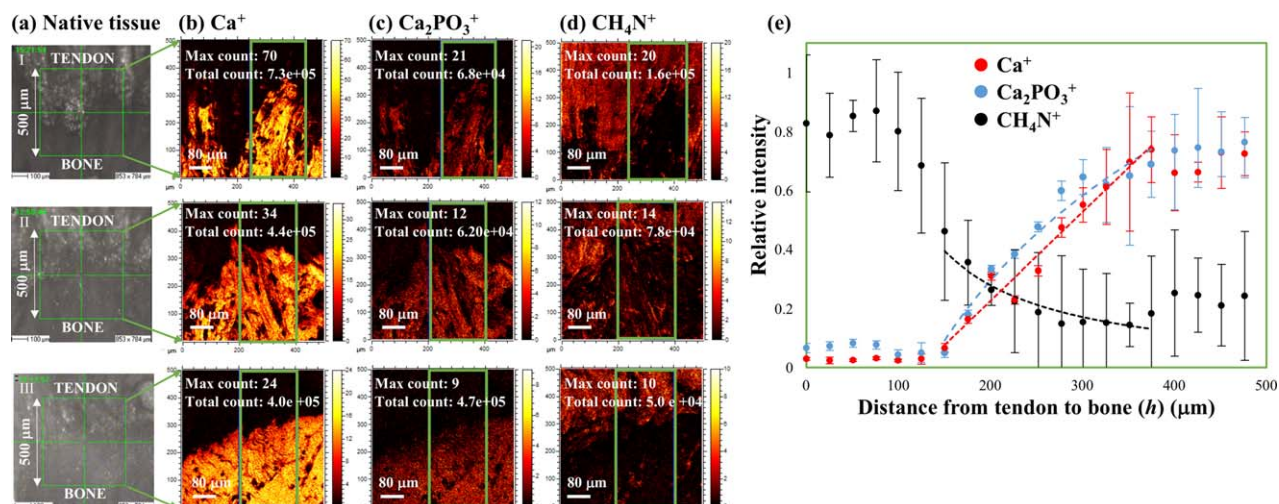
FIGURE 4. High resolution TOF images (500 × 500 μm) for (a) samples I, II, and III showing relative intensity distribution for (b) Ca^+ ions (sputtering was employed to destroy organic molecular fragments [$C_3H_4^+$] in the spectral neighborhood of Ca^+ ions), (c) apatite fragment $Ca_2PO_3^+$, and (d) collagen protein fragment CH_4N^+. (e) The relative concentration of each species across an insertion is calculated over the demarcated 200 × 500 μm area. The variation of Ca^+ follows a linear trend concurring with previous results from Raman microprobing.[13] The decrease in CH_4N^+ from the tendon to the insertion indicates a drop in type I collagen content in the fibrocartilaginous insertion zone.[2,3]

Figure 2(d). This corresponds to a fiber orientation angle (α) of 177° (87° + 90° = 177°) in Figure 2(b). Similarly, in the insertion region (I), the angle on the FFT (Θ) corresponding to a peak value of orientation distribution is 83° in Figure 2(d). This corresponds to a fiber orientation angle (α) of 173° in Figure 2(b). The fiber orientations [α in Fig. 3(c)] in the Y-Z plane of the tissue are measured in the same manner and compared with angle of orientation of the normal to the insertion boundary (β). Orientation index (OI), used as a measure of fiber dispersion, is calculated as the difference between the angles bounding the middle 50% area under the orientation distribution curve. Hence, an increase in randomization of fiber direction would correspond to shorter peaks and wider orientation indices.

Mineral distribution

TOF-SIMS analyses were conducted in the Analytical Instrumentation Facility at North Carolina State University using the ION-TOF SIMS 5 (ION TOF, Inc., Chestnut Ridge, NY) instrument equipped with a Bi_n^{m+}, ($n=1-5$, $m=1, 2$) liquid metal ion gun, Cs^+ sputtering gun, and electron flood gun for charge compensation.

For high lateral resolution mass spectral images acquired in this study, a burst alignment setting of 25 keV Bi^+ ion beam was used to raster a 500 × 500 μm area. The secondary ion mass spectral data were obtained over a range of mass/charge ratios from 0 to 160 with the mass scale calibrated using Ca^+, Ca_2Po^{3+}, and CH_4N^+. High intensity sputtering was employed to isolate the Ca^+ from organic fragments in its spectral neighborhood such as $C_3H_3^+$. Secondary ions were extracted at the detector by pre-acceleration to a 10 KeV kinetic energy at 2 kV and analyzed based on their respective flight times from the sample to the detector. Mass spectral peaks for Ca^+ and $Ca_2^+PO^{3+}$ fragments from calcium hydroxyapatite $Ca_{10}(PO_4)_6(OH)_2$

were chosen to track the apatite gradient across the insertion. The CH_4N^+ peak was chosen for the indication of collagen type I extracellular matrix protein[41] expressed predominantly in both pure tendon and pure bone zones as opposed to types II and X expressed only by the fibrocartilage transition.[48]

Analysis of secondary ion species. Three samples were studied for their molecular compositions by recording the respective counts of the secondary ions Ca^+, $Ca_2^+Po^{3+}$, and CH_4N^+ ejected from each 2 × 2 μm pixel area. Their respective relative intensity distributions are shown in Figure 4. Variation of the relative concentration of each species along the insertion is calculated over a prescribed 200 × 500 μm area in the region of interest for every sample spectral map as follows: Relative intensity of ion q at a distance h from the tendon end along the insertion is calculated by the count of ion q at h within a prescribed 200 μm width divided by the total count within the 200 × 500 μm insertion area; q stands for any of the analyzed secondary ion species from Ca^+, $Ca_2^+Po^{3+}$, and CH_4N^+, and h stands for the distance from the tendon end ranging from 0 to 500 μm. The count of each species is only a qualitative measure of its concentration on the test surface and is factored by the ionization potentials of each species.

RESULTS AND DISCUSSION

Through histological image analyses we examined the microstructure of 3D tendon-bone insertion tissue along its two orthogonal planes and obtained fiber orientation distributions across and along the insertion boundary.

Immunohistology results showing three-dimensional collagen structure are summarized in Figure 1. Optical microscopy images (400× magnification, water immersion) of H&E and VVG-stained sections of horizontal plane (X-Z

plane) in Figure 1(b) show variation in fiber organization through the depth of the insertion (along Y). Results suggest that global fiber orientations on all planes are centered around the direction of the physiological tension. This observation is supported by close proximity of mean orientation angles at the tendon, insertion, and bone regions as shown later in Figure 2(d). The images reveal the insertion tissue to be planar collagenous but not multilayered in terms of the fiber orientation. As previously noted,[6] sections at mid-depth [1200 μm, Fig. 1(b)] reveal maximum fiber density, the least amount of dispersion, and the least cellular circularity, while closer to the surface there is lower fiber density and organization, accompanied by the increased presence of proteoglycans and cellular circularity.

Variations in collagen structures along the medio-lateral direction (along X) are shown through microscopy images of H&E and VVG stained sections in the sagittal planes (Y-Z plane) of the tissue, respectively [Fig. 1(c,d)]. Results suggest the insertion boundary of the digital flexor tendon is a curved surface in the sagittal plane accompanied by the rotation of collagen fibers from the direction of the tendon axis toward the normal to the tidemark at each point on the boundary. Gradual rotation of collagen fibers away from the tendon axis at the point of insertion is qualitatively examined and results are presented in Figure 3.

Fiber orientation gradation across insertion regions on the horizontal plane (X-Z plane) is studied quantitatively through image analyses of histological data as summarized in Figure 2. Fluorescent imaging of the mid-depth (1200 μm) horizontal plane (X-Z plane) [Fig. 2(a): H&E staining, GFP fluorescence filter set with excitation wavelength = 450–490 nm and emission wavelength = 500–550 nm, 40× objective, water immersion] was used to selectively crop out images from regions of interest, namely pure bone, insertion, and pure tendon, as shown in Figure 2(b), and FFT was performed using a custom MATLAB code.[31] Results of FFT shown in Figure 2(c) clearly indicate gradation in the directionality of fiber orientation from the bone to the tendon region. Although the angle corresponding to peak values of orientation distribution is maintained across insertion, the progressive increase in the circularity of the FFT image from the tendon to the bony end is a reflection of the gradual decrease in the degree of anisotropy. This is in clear agreement with previous results from polarized light microscopy which also concluded that there is increased dispersion in fiber orientation at the bony end.[6] Angular distribution of FFT image pixels [indicated as Θ in Fig. 2(c)] is obtained as a measure of the collagen fiber orientation distribution in each of the three regions of bone, insertion, and tendon, and the results are presented in Figure 2(d). Thus, the orientation distribution of FFT at a given angle (Θ) indicates the associated number of frequencies in the frequency domain (or number of white pixels in the FFT oriented at Θ). The direction perpendicular to fiber orientation on the image would correspond to a higher number of associated frequencies and hence higher "orientation distribution." The OI predictably increases from the tendon to the insertion to the bone, suggesting a decrease in the

directionality, that is, decreases in the anisotropy of the fiber direction.

An important factor in the graded structure of the insertion tissue arises from the fact that collagen fibers from a strictly unidirectional tendon tissue insert onto a curved 2D bone surface. This gives rise to the need for collagen fiber reorientation at the insertion. We investigated the angle of rotation of fibers with respect to physiological axis in the sagittal plane (Y-Z plane) section shown in Figure 3(a). By performing FFT of insertion images at various points along the tidemark, we compared the mean angle of fiber orientation [indicated as α in Fig. 3(c) and shown as shaded bars in Fig. 3(d)] against the angle of inclination of the normal to the curved boundary [indicated as β in Fig. 3(b) and shown as orange bars in Fig. 3(d)]. The results indicate that the normal to the insertion boundary (that is, the transition from tendon to bone or vice-versa) is not necessary parallel with the collagen fiber orientation α of tendon tissue [Fig. 3(d)]. Current surgical procedures for reattachment of tendon to bone often fail,[49–53] owing to the unique transitional fiber orientation or rotation along the insertion boundary not being faithfully reconstructed. Our results suggest that to successfully regenerate the tendon-to-bone transition, it is of importance to have a complete understanding of α and β variations (or relationships) along the insertion boundary; it could be one of key factors enabling advanced treatments for tendon-to-bone healing.

In previous studies,[2,3,6] the four regions of the insertion were qualitatively discretized using optical microscopy, and collagen fiber orientation was measured using polarized light microscopy. The latter takes advantage of inherent tissue birefringence, where a rotating stage is needed to capture the extinction angle as an indication of the fiber direction. The polarized microscopy measurements showed the collagen orientation in rat shoulder insertions to be consistent in the tendon and bone insertion regions, with the distribution being less dispersed in the tendon side. Implementing the FFT method showed the same variation in fiber distribution across the insertion as the polarized light microscopy measurements, demonstrating its accuracy alongside ease of implementation. However, an important limitation in the FFT-based method is the indistinguishability of collagen fibers against other fibers such elastin, or other stained features on the image. Also, crimping in the fibers leads to the loss of high frequency data in the FFT images. It may be useful to perform image analysis in stretched configurations of fibers and also to investigate the fiber rotation model under various biaxial tension protocols. Further, elastin fibers being the other important structural component in the tendon connective tissue, their distribution across the insertion may be quantified as part of fiber study.

Another objective of the study was to track the gradation of mineralization along the insertion and to provide spatially continuous, high resolution mapping of the molecular fragments of apatite and collagen protein using TOF-SIMS as summarized in Figure 4. High resolution TOF-SIMS images were obtained over 500 × 500 μm areas of three

frozen insertion section samples as shown in Figure 4a. Intensity distributions for Ca^+ and $Ca_2PO_3^+$ [Fig. 4(b,c), respectively] fragments look qualitatively identical, indicative of a common source of calcium hydroxyapatite $Ca_{10}(PO_4)_6(OH)_2$. "Total count" indicated in Figures 4(b–d) signifies the number of secondary ions captured in the TOF-SIMS detector and "maximum count" indicates the number of entities detected per 2×2 μm pixel area. The count of each entity detected is hence a function of both its actual concentration as well as its ionization potential. The count of Ca^+ is one order of magnitude higher than that of $Ca_2PO_3^+$, in spite of their identical spatial distributions evident from Figure 4(b,c). This is a consequence of fragmentation of $Ca_2PO_3^+$ to Ca^+ as a result of sputtering.

Variations in apatite concentration were examined based on the relative intensities of Ca^+ and $Ca_2PO_3^+$ across the insertion, calculated over a constant area of 200×500 μm to eliminate errors due to inter-sample variability. We reported linear gradation in mineralization across the insertion based on surface characterization by TOF-SIMS. This is consistent with previous Raman spectroscopic observations of the spatial variation of mineral-collagen content across murine supraspinatus insertions.[13,14]

We found the intensity distribution of the collagen type I extracellular matrix protein[32] using CH_4N^+ [Fig. 4(d)] to mirror the apatite distributions shown in Figure 4(b,c). This peak was chosen because it is predominantly expressed in both pure tendon and pure bone zones as opposed to types II and X which are only expressed by the fibrocartilage transition. The organic fragment $C_3H_4^+$ mirrors that of Ca^+ and $Ca_2PO_3^+$, showing a decreasing trend with respect to distance from the tendon end. Based on collagen type characterization studies,[2,3] drops in CH_4N^+ may indicate the fibrocartilaginous insertion zone. A previous study[2,3] suggested collagen type I distribution across tendon-bone insertions mirrors that of collagen type II. The former was expressed predominantly in the pure tendon and pure bone zones, with a dramatic decrease in the fibrocartilage. Since a second peak in collagen type I is not manifested at the bony end in this study, it may be that the elemental mappings are inclusive only of the fibrocartilage region beyond $\sim$150 μm from the tendon end in the test area. It may be useful to further characterize the intensity distributions of other extracellular matrix proteins corresponding to collagen types II and X to confirm this hypothesis.

Spectral analyses using TOF-SIMS provided simultaneous molecular mapping that could be directly used for the calculation of spatial concentration variations, replacing the tedious peak fitting methods associated with quantification of Raman spectra. Also, the discrepancies between choosing Raman peak intensities versus Raman peak areas are bypassed given that the precise count of each species is used for the quantification.[14] The present technique therefore provides a spatially continuous measurement for the entire sample area as opposed to pointwise spectral information, as in the case of Raman microprobing.

Wopenka et al.[31] found a wider gradient region of 100 μm as opposed to the 25 μm wide region found by Schwartz et al.[13] at the developing murine enthesis in rats. It is suggested that mineral gradient scales are expected to change with organism size based on the suggestion that matrix composition could possibly determine the transport and concentrations of mineralization inhibitors.[13] The 250 μm wide gradient region seen at the porcine digitor flexor tendon insertion in this study is $\sim$10 times the mature cell diameter in the fibrocartilage, as may be noted from the scale of Figure 1(b). This confirms the hypothesis that the gradient region scale is higher for larger organisms and much larger than a single cell diameter.[13]

The experiments of this study are performed on porcine tendon-to-bone insertions (that is, digital flexor tendon to coffin/pedal bone). Pigs are ideal models for the development of regenerative medicine strategies/processes due to their similar body size and physiology compared with humans. However, these results may vary for other joints, namely the supraspinatus and Achilles tendon insertions, based on dissimilarities in bone anatomy. Incorporation of tissues from other locations may also be valuable to this study.

CONCLUSION

The insertion forms a functionally graded interface between tendon and bone. This study addresses quantification of gradual changes in: (1) the orientation distribution of collagen fibers on two orthogonal planes and (2) the relative concentration of the organic and inorganic tissue components. We have implemented an FFT-based method for determining collagen organization from histological sections which is shown to be an efficient replacement for the elaborate polarized light microscopy method. This quantification of collagen fiber orientation and dispersion across an insertion in this study is verified against measurements from polarized light microscopy.[2,3,10]

Features at the micrometer scale are important factors in the axial and shear moduli of tissue within the tendon-to-bone insertion.[7] Spectral mapping and micrometer scale imaging of the insertion tissue was carried out using the TOF-SIMS technique to capture relative abundances of its biochemical components. Mineral volume fraction varies inhomogeneously, although it is approximately linear across the tendon-to-bone insertion tidemark. Similar compositional analysis of injured and healing tissues could help explain functional differences relative to that of healthy tissue. The combination of FFT and spectral analyses provides complementary information about the complex structural properties of the inhomogeneous tendon-bone insertion tissue, and these results overall can pose important considerations in developing structure- and constituent-based constitutive models and injury mechanisms under super-physiological loading conditions.

of the authors and do not necessarily reflect the views of the National Science Foundation.

REFERENCES

1. Schwartz AG, Lipner JH, Pasteris JD, Genin GM, Thomopoulos S. Muscle loading is necessary for the formation of a functional tendon enthesis. Bone 2013;55:44–51.
2. Thomopoulos S, Williams GR, Gimbel JA, Favata M, Soslowsky LJ. Variation of biomechanical, structural, and compositional properties along the tendon to bone insertion site. J Orthop Res. 2003;21:413–419.
3. Thomopoulos S, Williams GR, Soslowsky LJ. Tendon to bone healing: Differences in biomechanical, structural, and compositional properties due to a range of activity levels. J Biomech Eng Trans ASME 2003;125:106–113.
4. Thomopoulos S, Zampiakis E, Das R, Silva MJ, Gelberman RH. The effect of muscle loading on flexor tendon-to-bone healing in a canine model. J Orthop Res 2008;26:1611–1617.
5. Benjamin M, Kumai T, Milz S, Boszczyk BM, Boszczyk AA, Ralphs JR. The skeletal attachment of tendons - tendon "entheses". Comp Biochem Physiol Mol Integr Physiol 2002;133:931–945.
6. Benjamin M, Evans EJ, Copp L. The histology of tendon attachments to bone in man. J Anat 1986;149:89–100.
7. Genin GM, Kent A, Birman V, Wopenka B, Pasteris JD, Marquez PJ, Thomopoulos S. Functional grading of mineral and collagen in the attachment of tendon to bone. Biophys J 2009;97:976–985.
8. Lu HH, Thomopoulos S. Functional attachment of soft tissues to bone: development, healing, and tissue engineering. Annu Rev Biomed Eng 2013;15:201–226.
9. Thomopoulos S, Genin GM, Galatz LM. The development and morphogenesis of the tendon-to-bone insertion - What development can teach us about healing. J Musculoskelet Neuronal Interact 2010;10:35–45.
10. Thomopoulos S, Marquez JP, Weinberger B, Birman V, Genin GM. Collagen fiber orientation at the tendon to bone insertion and its influence on stress concentrations. J Biomech 2006;39:1842–1851.
11. Lu HH, Subramony SD, Boushell MK, Zhang XZ. Tissue engineering strategies for the regeneration of orthopedic interfaces. Ann Biomed Eng 2010;38:2142–2154.
12. Robertson DB, Daniel DM, Biden E. Soft-tissue fixation to bone. Am J Sports Med 1986;14:398–403.
13. Schwartz AG, Pasteris JD, Genin GM, Daulton TL, Thomopoulos S. Mineral distributions at the developing tendon enthesis. Plos One 2012;7:1–11.
14. Wopenka B, Kent A, Pasteris JD, Yoon Y, Thomopoulos S. The tendon-to-bone transition of the rotator cuff: A preliminary raman spectroscopic study documenting the gradual mineralization across the insertion in rat tissue samples. Appl Spectrosc 2008;62:1285–1294.
15. Genin GM, Hutchinson JW. Composite laminates in plane stress: Constitutive modeling and stress redistribution due to matrix cracking. J Am Ceram Soc 1997;80:1245–1255.
16. Williams ML. Stress singularities resulting from various boundary conditions in angular corners of plates in extension. J Appl Mech Trans ASME 1952;19:526–528.
17. Rieppo J, Hallikainen J, Jurvelin JS, Kiviranta I, Helminen HJ, Hyttinen MM. Practical considerations in the use of polarized light microscopy in the analysis of the collagen network in articular cartilage. Microsc Res Tech 2008;71:279–287.
18. Whittaker P, Canham PB. Demonstration of quantitative fabric analysis of tendon collagen using 2-dimensional polarized-light microscopy. Matrix 1991;11:56–62.
19. Billiar KL, Sacks MSA. Method to quantify the fiber kinematics of planar tissues under biaxial stretch. J Biomech 1997;30:1997.
20. Sacks MS, Billiar KB. Chapter 3: Biaxial mechanical behavior of bioprosthetic heart cusps subjected to accelerated testing. In: Gabbay S, Frater R, editors. Advances in Anticalcific and Antidegenerative Treatment of Heart Valve Bioprostheses. Austin: Silent Partners; 1997.
21. Sacks MS. Focus on materials with scattered light. Res Dev 1988;30:73–78.
22. Sacks MS, Gloeckner DC. Quantification of the fiber architecture and biaxial mechanical behavior of porcine intestinal submucosa. J Biomed Mater Res 1999;46:1–10.
23. Sacks MS, Smith DB, Hiester ED. A small angle light scattering device for planar connective tissue microstructural analysis. Ann Biomed Eng 1997;25:678–689.
24. Axer H, von Keyserlingk DG, Prescher A. Collagen fibers in linea alba and rectus sheaths - II. Variability and biomechanical aspects. J Surg Res 2001;96:239–245.
25. Hansen KA, Weiss JA, Barton JK. Recruitment of tendon crimp with applied tensile strain. J Biomech Eng Trans ASME 2002;124:72–77.
26. Franchi M, Fini M, Quaranta M, De Pasquale V, Raspanti M, Giavaresi G, Ottani V, Ruggeri A. Crimp morphology in relaxed and stretched rat Achilles tendon. J Anat 2007;210:1–7.
27. Tan HY, Chang YL, Lo W, Hsueh CM, Chen WL, Ghazaryan AA, Hu PS, Young TH, Chen SJ, Dong CY. Characterizing the morphologic changes in collagen crosslinked-treated corneas by Fourier transform-second harmonic generation imaging. J Cataract Refract Surg 2013;39:779–788.
28. Sander EA, Barocas VH. Comparison of 2D fiber network orientation measurement methods. J Biomed Mater Res A 2009;88a:322–331.
29. Sander EA, Stylianopoulos T, Tranquillo RT, Barocas VH. Image-based biomechanics of collagen-based tissue equivalents multi-scale models compared to fiber alignment predicted by polarimetric imaging. IEEE Eng Med Biol Magazine 2009;28:10–18.
30. Ayres C, Bowlin GL, Henderson SC, Taylor L, Shultz J, Alexander J, Telemeco TA, Simpson DG. Modulation of anisotropy in electrospun tissue-engineering scaffolds: Analysis of fiber alignment by the fast Fourier transform. Biomaterials 2006;27:5524–5534.
31. Engelmayr GC, Cheng MY, Bettinger CJ, Borenstein JT, Langer R, Freed LE. Accordion-like honeycombs for tissue engineering of cardiac anisotropy. Nat Mater 2008;7:1003–1010.
32. Polzer S, Gasser TC, Forsell C, Druckmullerova H, Tichy M, Staffa R, Vlachovsky R, Bursa J. Automatic Identification and validation of planar collagen organization in the aorta wall with application to abdominal aortic aneurysm. Microsc Microanal 2013;19:1395–1404.
33. Chow MJ, Turcotte R, Lin CP, Zhang YH. Arterial extracellular matrix: A mechanobiological study of the contributions and interactions of elastin and collagen. Biophys J 2014;106:2684–2692.
34. Schindelin J, Arganda-Carreras I, Frise E, Kaynig V, Longair M, Pietzsch T, Preibisch S, Rueden C, Saalfeld S, Schmid B, Tinevez JY, White DJ, Hartenstein V, Eliceiri K, Tomancak P, Cardona A. Fiji: an open-source platform for biological-image analysis. Nat Methods 2012;9:676–682.
35. Schneider CA, Rasband WS, Eliceiri KW. NIH Image to ImageJ: 25 years of image analysis. Nat Methods 2012;9:671–675.
36. Rezakhaniha R, Agianniotis A, Schrauwen JTC, Griffa A, Sage D, Bouten CVC, van de Vosse FN, Unser M, Stergiopulos N. Experimental investigation of collagen waviness and orientation in the arterial adventitia using confocal laser scanning microscopy. Biomech Model Mechanobiol 2012;11:461–473.
37. Weichsel J, Urban E, Small JV, Schwarz US. Reconstructing the orientation distribution of actin filaments in the lamellipodium of migrating keratocytes from electron microscopy tomography data. Cytometry Part A 2012;81a:496–507.
38. ChiuHuang C-K, Zhou C, Huang H-YS. In-situ imaging of lithium-ion batteries via the secondary ion mass spectrometry. ASME J Nanotechnol Eng Med 2014;5, pp. 021002-1-5.
39. Barofsky DF, Brinkmalm G, Hakansson P, Sundqvist BUR. Quantitative-determination of kinetic-energy releases from metastable decompositions of sputtered organic ions using a time-of-flight mass-spectrometer with a single-stage ion mirror. Int J Mass Spectrom Ion Process 1994;131:283–294.
40. Belu AM, Graham DJ, Castner DG. Time-of-flight secondary ion mass spectrometry: Techniques and applications for the characterization of biomaterial surfaces. Biomaterials 2003;24:3635–3653.
41. Brown BN, Barnes CA, Kasick RT, Michel R, Gilbert TW, Beer-Stolz D, Castner DG, Ratner B, Badylak SF. Surface characterization of extracellular matrix scaffolds. Biomaterials 2010;31:428–437.

42. Cersoy S, Richardin P, Walter P, Brunelle A. Cluster TOF-SIMS imaging of human skin remains: analysis of a South-Andean mummy sample. J Mass Spectrom 2012;47:338–346.

43. Layrolle P, Lebugle A. Characterization and reactivity of nanosized calcium phosphates prepared in anhydrous ethanol. Chem Mater 1994;6:1996–2004.

44. Lu HB, Campbell CT, Graham DJ, Ratner BD. Surface characterization of hydroxyapatite and related calcium phosphates by XPS and TOF-SIMS. Anal Chem 2000;72:2886–2894.

45. McDonnell LA, Piersma SR, Altelaar AFM, Mize TH, Luxembourg SL, Verhaert PDEM, van Minnen J, Heeren RMA. Subcellular imaging mass spectrometry of brain tissue. J Mass Spectrom 2005;40:160–168.

46. Nygren H, Johansson BR, Malmberg P. Bioimaging TOF-SIMS of tissues by gold ion bombardment of a silver-coated thin section. Microsc Res Tech 2004;65:282–286.

47. Ward AJ, Short RD. A Tofsims and Xps investigation of the structure of plasma polymers prepared from the methacrylate series of monomers. 2. The influence of the W/F parameter on structural and functional-group retention. Polymer 1995;36:3439–3450.

48. Galatz L, Rothermich S, VanderPloeg K, Petersen B, Sandell L, Thomopoulos S. Development of the supraspinatus tendon-to-bone insertion: Localized expression of extracellular matrix and growth factor genes. J Orthop Res 2007;25:1621–1628.

49. Thomopoulos S, Hattersley G, Rosen V, Mertens M, Galatz L, Williams GR, Soslowsky LJ. The localized expression of extracellular matrix components in healing tendon insertion sites: an in situ hybridization study. J Orthop Res 2002;20:454–463.

50. Galatz LM, Sandell LJ, Rothermich SY, Das R, Mastny A, Havlioglu N, Silva MJ, Thomopoulos S. Characteristics of the rat supraspinatus tendon during tendon-to-bone healing after acute injury. J Orthop Res 2006;24:541–550.

51. Wong MWN, Qin L, Lee KM, Leung KS. Articular cartilage increases transition zone regeneration in bone-tendon junction healing. Clin Orthop Relat Res 2009;467:1092–1100.

52. Wong MWN, Tai KO, Lee KM, Qin L, Leung KS. Bone formation and fibrocartilage regeneration at bone tendon junction with allogeneic cultured chondrocyte pellet interposition. J Bone Miner Res 2007;22:1128–1129.

53. Rodeo SA, Arnoczky SP, Torzilli PA, Hidaka C, Warren RF. Tendon-healing in a bone tunnel. A biomechanical and histological study in the dog. J Bone Joint Surg Am 1993;75:1795–1803.